

# Slotted Aloha with Capture for OWC-based IoT: Design and Analysis in Finite Block-Length Regime

Tijana Devaja, *Student Member, IEEE*, Milica Petkovic, *Member, IEEE*, Francisco J. Escribano, *Member, IEEE*, Čedomir Stefanović, *Senior Member, IEEE*, Dejan Vukobratovic, *Senior Member, IEEE*

**Abstract**—In this paper, we propose a Slotted ALOHA (SA)-inspired solution for an indoor optical wireless communication (OWC)-based Internet of Things (IoT) system. Assuming that the OWC receiver exploits the capture effect, we are interested in the derivation of error probability of decoding a short-length data packet originating from a randomly selected OWC IoT transmitter. The presented OWC system analysis rests on the derivation of the signal-to-noise-and-interference-ratio (SINR) statistics and usage of finite block-length (FBL) information theory, from which relevant error probability and throughput is derived. Using the derived expressions, we obtain numerical results which are further utilized to characterize the trade-offs between the system performance and the OWC system setup parameters. The indoor OWC-based system geometry plays an important role in the system performance, thus the presented results can be used as a guideline for the system design to optimize the performance of the SA-based random access protocol.

**Index Terms**—Finite Block-Length, Error Probability, Internet of Things, Optical Wireless Communications, Random Access, Slotted ALOHA.

## I. INTRODUCTION

The domain of optical wireless communications (OWC) is gaining attention as a complementary technology able to offload massive wireless traffic in indoor environments, relaxing the challenges posed by the spectrum crunch experienced by current RF-based technologies. In fact, spectrum shortage is promoting a surge of research aimed at exploiting higher frequency bands for wireless communications, ranging from millimeter-wave, via terahertz to optical (infrared or visible) bands [2]–[5]. Each of these possibilities appears to be well suited for specific environments and applications, and the ongoing research trends point towards a combination of strategies to meet the requirements of ever-increasing number of IoT devices.

Resorting to specific bands to establish communication links for a given application is only part of the context. If we focus on the needs of an IoT wireless framework where the communication medium is shared, granting fair access to the resources and guaranteeing the link quality in presence of possible interference is of paramount importance [6], [7]. The

nature of the foreseeable traffic generated by IoT devices adds to the challenges to be addressed: short data packets generated randomly, without centralized coordination. In this context, well designed random access (RA) protocols are key to keeping the system working appropriately [8]–[11]. In the last decades, we have witnessed a general trend where we do not forcibly avoid interference in wireless media, but try to get the best from it, while being even able to increase the capacity available from scarce spectrum resources (e.g. by resorting to spread spectrum or MIMO spatial multiplexing techniques). In the domain of access schemes, the same principle is being applied, for example in form of the so-called capture effect, where user data can be recovered under specific conditions even in presence of concurrent transmissions in the medium. This can alleviate the need for strict collision-avoidance RA protocols and opens the road to designing simple and efficient RA schemes, for example, inspired in the ALOHA protocol. More specifically, slotted ALOHA (SA) seems to be an interesting alternative where the application of the capture effect can help in increasing the overall throughput [12]–[14].

One of the scenarios where IoT deployments are being envisaged include indoor spaces comprising large rooms without dividing walls (like warehouses or open-plan offices), where a large quantity of devices will be collecting, processing and sending data to a number of access points. In this situation, the usage of RF links could lead to a disabling level of interference and a high probability of packet loss due to collisions. Although facing limited coverage, transmission technologies based on OWC can help to tackle these issues. In fact, by using OWC links, there will be no interference across walls, and a small scale indoor cellular network could be designed to cover the whole space with minimal coverage overlapping, thus maximizing the overall throughput.

The OWC systems have been studied in the recent literature as a potential indoor IoT solution in current and upcoming generation of the communication technologies [15]–[21]. Moreover, the OWC-based IoT systems with different uplink RA approaches with sporadic and varying device activity were analyzed in [22]–[25]. More precisely, [22] analyzed the uplink multi-receiver OWC system in the context of massive IoT application, where coded SA approach with successive interference cancellation was adopted. In [23], Zhao *et al.* analyzed multi-packet reception (MPR)-aided VLC system and introduced a novel quality of service (QoS)-driven non-carrier sensing RA scheme. The same authors investigated the MPR capable uplink OWC system with heterogeneous statistical delay QoS guarantees for ALOHA-based RA [24].

This paper was presented in part at the 17th International Symposium On Wireless Communication Systems (ISWCS) 2021 [1].

T. Devaja, M. Petkovic and D. Vukobratovic are with University of Novi Sad, Faculty of Technical Science, 21000 Novi Sad, Serbia (e-mails: tijana.devaja@uns.ac.rs; milica.petkovic@uns.ac.rs; dejanv@uns.ac.rs).

F. J. Escribano is with Universidad de Alcalá, Alcalá de Henares, Spain (e-mail: francisco.escribano@uah.es).

Č. Stefanović is with Aalborg University, Aalborg, Denmark (e-mail: cs@es.aau.dk).

An optical camera communication based on ALOHA RA scheme was analyzed in [25], where the access probability of each terminal was utilized to perform the access fairness and system throughput rate optimization.

The design and optimization of an RA scheme based on the capture effect for an OWC-based IoT indoor network requires the analysis and evaluation of the signal-to-interference ratio (SINR). From SINR statistics one can derive the error probability affecting the captured data packets, protected by an appropriate channel code, thereby determining the system performance. Besides the SINR characterization in this kind of environment and how it is affected by the meaningful parameters of the system, the error and coding rate analysis is still lacking in open literature. Information theory has traditionally focused on data transmission reliability through noisy channels that may be achievable for large channel coded data block lengths, but the fact is that for IoT applications, we are dealing with short block-length transmissions. In this sense, the so-called finite block-length (FBL) information theory [26] provides us with the appropriate tools to analyze what relates to error probability estimation and the corresponding maximum achievable rate for a given target quality.

The aim of this paper is a detailed study of the SINR derivation of the OWC-based IoT with capture effect. Furthermore, the main novelty of this paper is the addition and development of the error probability analysis based on FBL theory, as well as the evaluation of the impact in the overall system performance of the main parameters of the OWC-based IoT framework. These contributions are particularly important because a real-world IoT network deployment requires for its design and assessment the suitable analysis tools in order not only to appropriately set its physical parameters, but also how to configure the access protocols for optimal performance.

The paper is structured as follows. In Section II, we review the system model and set the main hypothesis. In Section III, we derive the SINR statistics for the proposed situation. In Section IV, we analyze the error probability and channel coding rate based on the FBL regime approach. In Section V, we present and discuss numerical results and, finally, in Section VI, we close the paper with the main conclusions.

## II. SA-BASED INDOOR OWC IoT: A SYSTEM MODEL

The context of this work comprises a communication scenario where a total of  $U$  IoT devices equipped with OWC transmitters contend to access a common OWC access point (AP). The transmitting devices are uniformly placed on a horizontal plane, while the OWC AP is located at the ceiling, in a fixed location (see Fig. 1). This situation reflects well an open-plan office space with IoT devices placed on tables or other furniture. The SA protocol [10] is considered for this kind of uplink transmission. Each IoT device is active for transmission with probability  $p_a$  in every slot, independently of its activity in other slots, and the activity of other devices during the same slot period. If a user is active in a slot, it transmits a fixed-length packet of finite (short) blocklength. The number of active users in a given slot is denoted by  $0 \leq U_a \leq U$ , and it is assumed to be a fixed (but unknown)

parameter. We will derive expressions in our analysis as a function of  $U_a$ , and then provide averages over it. In the sequel, we assume Bernoulli arrivals for the activation of the IoT devices, in order to model the distribution of  $U_a$ .

The IoT devices use infrared (IR) LED sources, and the physical transmission employs a simple intensity-modulation (IM) binary-format signaling (e.g., non-return-to-zero on-off keying, OOK). All the devices transmit with the same optical power regardless of any other condition. The OWC photo-detector (PD) receiver performs direct detection (DD) of the arriving light intensity [3]. At any given slot, the light intensity impinging the OWC PD receiver comprises the contribution of the  $U_a$  active users plus the background radiation noise. Assuming that the PD is working in a linear regime (which is a standard and reasonable approximation in practical situations), the received signal after the conversion to the electrical domain (and prior to decoding) can be modeled as

$$y(t) = \sum_{i=1}^{U_a} P_t \eta h_i x_i(t) + n(t) \quad (1)$$

where  $x_i(t)$ ,  $i = 1, \dots, U_a$ , is the unit-power signal waveform from the  $i$ -th user,  $P_t$  is the transmitted optical power,  $\eta$  the optical-to-electrical conversion coefficient,  $h_i \geq 0$  the optical gain from the  $i$ -th user to the AP, while  $n(t)$  is an instance of additive white Gaussian noise with power spectral density  $N_0/2$ . This kind of noise process adequately models the distorting effects of the optical background radiation plus the receiver thermal noise, and contributes to the signal-to-noise balance with a noise power  $\sigma_n^2 = N_0 B$ , where  $B$  is the system noise bandwidth.

Under these conditions, if a slot contains transmissions from two or more users ( $U_a \geq 2$  for such slot), a packet collision takes place. In that case, by exploiting capture effect, the OWC AP receiver of our setup will try to decode the slot, in contrast with the classical SA protocol. We are interested in the probability that the receiver succeeds in decoding a randomly selected user among the set of active ones. For convenience, and without loss of generality, we assume that the index of such user (denoted as our *reference user* henceforth) corresponds to  $i = 1$ . Therefore, the received signal (1) can

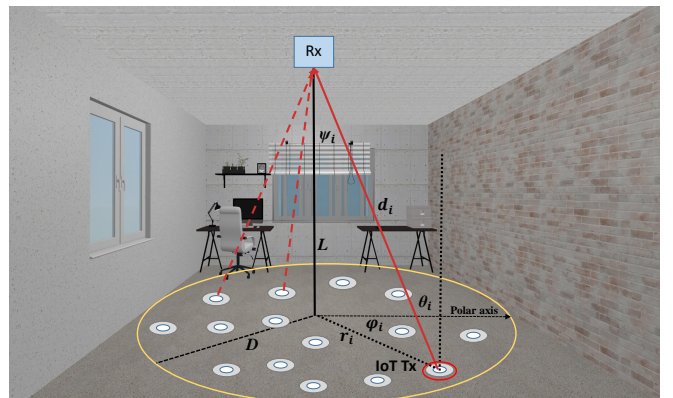


Fig. 1. OWC-based indoor IoT system model.

be rewritten as

$$y(t) = P_t \eta h_1 x_1(t) + \sum_{i=2}^{U_a} P_t \eta h_i x_i(t) + n(t) \quad (2)$$

where  $x_1(t)$  is the signal waveform from the reference user,  $h_1 \geq 0$  is the corresponding optical channel gain, and the summation term represents the interference contribution from all other active users.

Based on (2), the signal-to-interference noise ratio (SINR) experienced by the reference user can be readily written as

$$\begin{aligned} \text{SINR} &= \frac{P_t^2 \eta^2 h_1^2}{\sum_{i=2}^{U_a} P_t^2 \eta^2 h_i^2 + \sigma_n^2} \\ &= \frac{\gamma_1}{\sum_{i=2}^{U_a} \gamma_i + 1} = \frac{\gamma_1}{\gamma_1 + 1} \end{aligned} \quad (3)$$

where

$$\gamma_1 = \frac{P_t^2 \eta^2 h_1^2}{\sigma_n^2}, \quad \gamma_i = \frac{P_t^2 \eta^2 h_i^2}{\sigma_n^2}, \quad \gamma_1 = \sum_{i=2}^{U_a} \gamma_i. \quad (4)$$

This SINR depends not only on the number of active users, but also on the specific placements of the IoT devices with respect to the OWC AP (which, in turn, determines the specific values of the optical path gains,  $h_i$ ). In the next section, we derive the statistics for the SINR observed by a randomly selected active user, based on specific hypothesis and choices over the system setup and optical parameters.

### III. SINR STATISTICS FOR SA-BASED OWC IoT

As shown in Fig. 1, we assume that the devices are randomly and uniformly distributed over the indoor circular coverage area of radius  $D$  within the same horizontal plane. The OWC AP is positioned at a height  $L$  above said plane, over the center of the circle. The location of the  $i$ -th user with respect to the OWC AP is determined with the angle  $\theta_i$  (angle of irradiance), the angle  $\varphi_i$ , and the radius  $r_i$  in the polar coordinate plane. The angle of incidence into the AP is denoted as  $\psi_i$ , and the Euclidean distance between the corresponding LED transmitter and the PD receiver is denoted as  $d_i$ . The optical channel gain of the LoS link between the  $i$ -th device and the PD receiver can be determined as [27]

$$h_i = \frac{A_r (m+1) R_r}{2\pi d_i^2} \cos^m(\theta_i) T_s g(\psi_i) \cos(\psi_i), \quad (5)$$

where  $A_r$  is the surface area of the PD,  $R_r$  is the responsivity,  $T_s$  is the gain of the optical filter,  $g(\psi_i)$  is the response of the optical concentrator, and the factor  $m$  will be described in the sequel. The optical concentrator is modeled as  $g(\psi_i) = \zeta^2 / \sin^2(\Psi)$ , for  $0 \leq \psi_i \leq \Psi$ , where  $\zeta$  is the refractive index of the lens at the PD and  $\Psi$  denotes its field of view (FoV). Finally, the LED emission follows a generalized Lambertian radiation pattern with order  $m = -\ln 2 / \ln(\cos \Phi_{1/2})$ , where  $\Phi_{1/2}$  denotes the semi-angle at half illuminance<sup>1</sup> [3].

In this situation, if the surface of the PD receiver is parallel to the plane where the IoT devices are located, then  $\theta_i = \psi_i$ ,

<sup>1</sup>We assume that all LEDs are characterized by the same parameters, i.e.,  $m_i = m$  and  $\Phi_{1/2}^i = \Phi_{1/2}$  for  $\forall i$ .

$d_i = \sqrt{r_i^2 + L^2}$ ,  $\cos(\theta_i) = \frac{L}{\sqrt{r_i^2 + L^2}}$ , and equation (5) can be rewritten as

$$h_i = \frac{\mathcal{X}}{(r_i^2 + L^2)^{\frac{m+3}{2}}} \quad (6)$$

where  $\mathcal{X} = \frac{A_r(m+1)R_r}{2\pi} T_s g(\psi_i) L^{m+1}$  is a factor that does not depend on the specific placement of the IoT device, provided that the angle  $\psi_i$  lies below the PD FoV (a condition met for the values of  $D$  and  $L$  considered here).

As the IoT devices are distributed uniformly, the PDF of their radial distance  $r_i$  from the centre of the circle is [28]

$$f_{r_i}(x) = \frac{2x}{D^2}, \quad 0 \leq x \leq D. \quad (7)$$

By using expressions (6) and (7), and standard RV transformation techniques, the PDF of the optical channel gains,  $h_i$ , can be derived as

$$f_{h_i}(x) = \frac{2\mathcal{X}^{\frac{2}{m+3}}}{D^2(m+3)} x^{-\frac{m+5}{m+3}}, \quad h_{\min} \leq x \leq h_{\max}, \quad (8)$$

where  $h_{\min} = \frac{\mathcal{X}}{(D^2+L^2)^{\frac{m+3}{2}}}$  and  $h_{\max} = \frac{\mathcal{X}}{L^{m+3}}$ .

The PDF of  $\gamma_i$ , defined previously in (4), can be similarly derived as [28]

$$f_{\gamma_i}(x) = \frac{(\mu\mathcal{X}^2)^{\frac{1}{m+3}}}{D^2(m+3)} x^{-\frac{m+4}{m+3}}, \quad \gamma_{\min} \leq x \leq \gamma_{\max}, \quad (9)$$

where  $\gamma_{\min} = \frac{\mu\mathcal{X}^2}{(D^2+L^2)^{m+3}}$ ,  $\gamma_{\max} = \frac{\mu\mathcal{X}^2}{L^{2(m+3)}}$ , and  $\mu = \frac{P_t^2 \eta^2}{\sigma_n^2}$ .

To get the statistical characterization of the overall SINR, we can use the characteristic function (CF) approach [29]. In this case, the CF of  $\gamma_i = \frac{P_t^2 \eta^2 h_i^2}{\sigma_n^2}$  can be derived via (9) as

$$\begin{aligned} \varphi_{\gamma_i}(t) &\triangleq \mathbb{E}[e^{jt\gamma_i}] = \int_{-\infty}^{\infty} e^{jtx} f_{\gamma_i}(x) dx \\ &= \frac{(\mu\mathcal{X}^2)^{\frac{1}{m+3}}}{D^2(m+3)} \int_{\gamma_{\min}}^{\gamma_{\max}} x^{-\frac{m+4}{m+3}} e^{jtx} dx = \frac{(\mu\mathcal{X}^2)^{\frac{1}{m+3}}}{D^2(m+3)}, \\ &\times \left( \Gamma\left(-\frac{1}{m+3}, -jt\gamma_{\min}\right) - \Gamma\left(-\frac{1}{m+3}, -jt\gamma_{\max}\right) \right), \end{aligned} \quad (10)$$

where  $\Gamma(\cdot, \cdot)$  is the upper incomplete gamma function [30, (8.35)].

#### A. Contribution to the SINR Statistics from the Reference User

For the reference user, the PDF of  $\gamma_1$  can be calculated as a specific case of equation (9), which we rewrite here for clarity

$$f_{\gamma_1}(x) = \frac{(\mu\mathcal{X}^2)^{\frac{1}{m+3}}}{D^2(m+3)} x^{-\frac{m+4}{m+3}}, \quad \gamma_{\min} \leq x \leq \gamma_{\max}. \quad (11)$$

#### B. Contribution to the SINR Statistics from the Interfering Users

The channel gains  $h_i$  (thus also  $\gamma_i$ ) are independent and identical distributed (i.i.d.) RVs when the IoT device locations

are also i.i.d. RVs. In this case, the CF of  $\gamma_I = \sum_{i=2}^{U_a} \gamma_i$  can be determined as [29]

$$\begin{aligned} \varphi_{\gamma_I}(t) &\triangleq \mathbb{E} [e^{jt\gamma_I}] = \mathbb{E} [e^{jt \sum_{i=2}^{U_a} \gamma_i}] = \mathbb{E} \left[ \prod_{i=2}^{U_a} e^{jt\gamma_i} \right] \\ &= \prod_{i=2}^{U_a} \mathbb{E} [e^{jt\gamma_i}] = \prod_{i=2}^{U_a} \varphi_{\gamma_i}(t) = \varphi_{\gamma_i}^{U_a-1}(t) \end{aligned} \quad (12)$$

where the CF of  $\gamma_i$  is defined in (10). The PDF of  $\gamma_I$  can be derived as

$$\begin{aligned} f_{\gamma_I}(x) &= \frac{1}{2\pi} \int_{-\infty}^{\infty} e^{-jtx} \varphi_{\gamma_I}(t) dt \\ &= \frac{1}{2\pi} \int_{-\infty}^{\infty} e^{-jtx} \varphi_{\gamma_i}^{U_a-1}(t) dt, \end{aligned} \quad (13)$$

for  $\gamma_{\min}^{U_a-1} \leq x \leq \gamma_{\max}^{U_a-1}$ .

### C. Overall SINR Statistics for the Reference User

As an intermediate step, we derive the PDF of the RV defined as  $\lambda = \gamma_I + 1$ , namely

$$\begin{aligned} f_{\lambda}(\lambda) &= \frac{f_{\gamma_I}(\gamma_I)}{\left| \frac{d\lambda}{d\gamma_I} \right|} = f_{\gamma_I}(\lambda - 1) \\ &= \frac{1}{2\pi} \int_{-\infty}^{\infty} e^{-jt(\lambda-1)} \varphi_{\gamma_i}^{U_a-1}(t) dt, \end{aligned} \quad (14)$$

for  $\gamma_{\min}^{U_a-1} + 1 \leq \lambda \leq \gamma_{\max}^{U_a-1} + 1$ . Since  $\gamma_I$  and  $\gamma_I$  are independent RVs, their joint PDF is  $f_{\gamma_I, \lambda}(x, \lambda) = f_{\gamma_I}(x) f_{\lambda}(\lambda)$ . The PDF of the SINR  $= \frac{\gamma_I}{\gamma_I + 1}$  of the reference user, conditioned on the total number of active users  $U_a$ , can be derived as follows [31]

$$f_{\text{SINR}}(x|U_a) = \int_{-\infty}^{\infty} |\lambda| f_{\gamma_I}(x\lambda) f_{\lambda}(\lambda) d\lambda, \quad (15)$$

where  $f_{\gamma_I}(x)$  and  $f_{\lambda}(\lambda)$  are previously defined in equations (11) and (14), respectively. After replacing (11) and (14) in equation (15), since  $\lambda > 0$ , the PDF can be derived as

$$\begin{aligned} f_{\text{SINR}}(x|U_a) &= \frac{(\mu\mathcal{X}^2)^{\frac{1}{m+3}}}{2\pi D^2(m+3)} x^{-\frac{m+4}{m+3}} \\ &\times \int_{\gamma_{\min}^{U_a-1}+1}^{\gamma_{\max}^{U_a-1}+1} \lambda^{-\frac{1}{m+3}} \left( \int_{-\infty}^{\infty} e^{-jt(\lambda-1)} \varphi_{\gamma_i}^{U_a-1}(t) dt \right) d\lambda \end{aligned} \quad (16)$$

where  $\varphi_{\gamma_i}(t)$  is the CF previously defined in equation (10). The statistics of the SINR will allow us to derive the error probability for our proposed setup in the next Section.

The CDF of the SINR of the reference user, conditioned on  $U_a$ , can be derived as

$$F_{\text{SINR}}(\gamma|U_a) = \int_0^{\gamma} f_{\text{SINR}}(x|U_a) dx. \quad (17)$$

## IV. ERROR PROBABILITY AND THROUGHPUT FOR SA VIA FBL APPROACH

Goal of information theory is to quantify the extent to which reliable communication is possible over a noisy channel. A code of size  $N$  and block length  $n$  allows communication of

one of  $N$  messages via  $n$  uses of the channel. The fundamental trade-off between these quantities and the reliability of communication, is captured by  $N_{\epsilon}(n)$ - the largest size of code with error probability  $\epsilon$  (for equiprobable messages). Code rate  $R = \log_2 n/N$  is commonly used instead of exponentially increasing size  $N$  of the code. Thus investigating the maximum code rate  $R_{\epsilon}(n)$  that still allows communication with  $n$  channel uses while providing reliability  $\epsilon$  is the central question of FBL theory.

Building upon the classical Shannon's asymptotic results, Polyanskiy, Poor, and Verdú showed that for the AWGN channel with capacity  $C(\gamma) = \log_2(1 + \gamma)$ , where  $\gamma$  denotes the SNR, the maximal achievable rate, for the decoding error probability  $\epsilon$ , can be tightly approximated as [26]

$$R = C(\gamma) - \sqrt{\frac{V_{\text{AWGN}}(\gamma)}{n}} Q^{-1}(\epsilon) + O\left(\frac{\log n}{n}\right) \quad (18)$$

where  $Q^{-1}(\cdot)$  denotes the inverse of the Gaussian Q-function defined as  $Q(x) = \int_x^{\infty} \frac{1}{\sqrt{2\pi}} e^{-\frac{t^2}{2}} dt$ , while the channel dispersion is defined as

$$V_{\text{AWGN}}(\gamma) = \left(1 - \frac{1}{1 + \gamma^2}\right) \log_2^2(e). \quad (19)$$

We are interested in the error probability of decoding a short-length data packet of a single active user by taking into account interference contribution from all other active users in a given slot (see (3)). Using standard "treat interference as noise" approximation, one can treat interference as an additional Gaussian noise. Strictly speaking, however, aggregate interference does not obey Gaussian statistics (to achieve 18, transmitters need to use a non-Gaussian codebook), meaning that the OWC receiver experiences non-Gaussian interference. More precise approximation is provided in [32] assuming a non-Gaussian interference and nearest-neighbor decoding. In this case, the channel dispersion derived in [32] (see also [33]) should be applied instead of (19), i.e.,

$$V(\gamma) = \frac{2\gamma}{1 + \gamma} \log_2^2(e). \quad (20)$$

For  $n > 100$  channel uses, the item  $O(\frac{\log n}{n})$  in (18) can be omitted, thus the achievable rate can be well approximated as

$$R \approx C(\gamma) - \sqrt{\frac{V(\gamma)}{n}} Q^{-1}(\epsilon). \quad (21)$$

The approximation (21) is established by characterizing the asymptotic behavior of analytically tractable achievability and converse bounds (see [26], Sec. III).

For the system setup considered in this paper, based on (21) and adopting that SINR =  $\gamma$ , the decoding error probability can be tightly approximated as

$$\epsilon(\gamma, U_a) = Q\left(\sqrt{\frac{n}{V(\gamma)}}(C(\gamma) - R)\right) \quad (22)$$

For the sake of clarity, in the above equation, we make the dependence of error probability  $\epsilon(\gamma, U_a)$  on the number of active users  $U_a$  explicit, although this dependence is implicit through the dependence of the SINR statistics  $\gamma(U_a)$  on

the number of active users  $U_a$ . By conditioning the error probability over the SINR, we get

$$\epsilon(U_a) = \int_{\gamma} \epsilon(\gamma, U_a) f_{\text{SINR}}(\gamma|U_a) d\gamma. \quad (23)$$

where  $f_{\text{SINR}}(\gamma|U_a)$  is previously derived in (16). Finally, the unconditional error probability  $P_e$  can be derived as

$$\epsilon = \sum_{u \geq 1} \epsilon(U_a) \mathbb{P}[U_a = u], \quad (24)$$

where  $\mathbb{P}[U_a = u] = \binom{U}{u} p_a^u (1 - p_a)^{U-u}$ .

Considering FBL regime with the maximal achievable rate  $R$ , and the probability that the packet is decoded at the OWC system at each slot derived previously as in (24), overall throughput is defined as

$$T = R(1 - \epsilon)(1 - (1 - p_a)^U), \quad (25)$$

where  $1 - (1 - p_a)^U$  represents the probability that at least one user is active during the slot.

## V. NUMERICAL RESULTS AND DISCUSSION

In this section, using the analysis presented in Sec. III and Sec. IV, we focus on the design and performance evaluation of an indoor OWC IoT system. Numerical results are obtained by adopting the following values for the main parameters: the OWC IoT device transmitted optical power is  $P_t = 30$  mW, the OWC AP receiver PD surface area equals to  $A_r = 1$  cm<sup>2</sup>, its responsivity is  $R_r = 0.4$  A/W, the FoV of the PD receiver is  $90^\circ$ , while the optical filter gain is  $T_s = 1$ , and the refractive index of the lens at a PD is  $\zeta = 1.5$ . Furthermore, the receiver optical-to-electrical conversion efficiency is  $\eta = 0.8$ , while the noise power spectral density takes a value  $N_0 = 10^{-21}$  W/Hz, and the system bandwidth is chosen to be  $B = 200$  kHz.

Since both the PDF and CDF of the SINR in (16) and (17), respectively, are given in integral form, presented results are obtained by numerical computation performed through the FFT algorithm implemented in MATLAB. Fig. 2 presents the

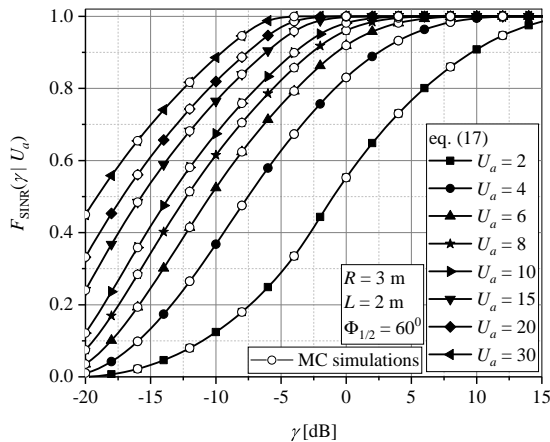


Fig. 2. CDF of the SINR of the reference user conditioned on  $U_a$ ,  $F_{\text{SINR}}(\gamma|U_a)$ .

CDF of the SINR derived in (17), where numerical computations are confirmed through Monte Carlo (MC) simulations.

Fig. 3 depicts the error probability of considered OWC system in FBL regime in dependence on the OWC AP height  $L$  for various levels of error protection parametrized by the code rate  $R$ . As expected, increasing of  $R$  will result in the error protection performance deterioration. Additionally, two different values of radius  $D$  are considered. When radius  $D$  is greater, the OWC IoT users will be distributed over a wider area, which will increase the chance that each of them is far distant from the OWC AP. Greater distance of OWC users from the AP leads to the reduced received power, and consequently the overall SINR is lower. This will affect the capture probability, thus the error probability of considered system will be increased when  $D$  is greater. From Fig. 3, it can be concluded that the impact of the rate value on the error probability performance is diminished when the radius  $D$  is greater. Consequently, the geometric setup of the OWC based IoT framework will have impact on the system performance behavior in FBL regime.

Fig. 4 shows the throughput dependence on the activation probability  $p_a$  for different number of OWC-based IoT devices  $U$  in the room and different values of radius  $D$ . Similarly as in previous Fig. 3, greater value of radius  $D$  leads to the worse system performance, i.e., lower throughput of considered system in this case. Greater activation probability  $p_a$ , as well as total number of users  $U$ , brings to the greater number of active users in OWC IoT system in a slot. The number of active IoT devices determines the overall SINR, which has impact on the capture effect procedure. From Fig. 4, it can be observed that the maximal value of the system throughput exists for the optimal value of  $p_a$ . This optimal value is dependent on the total number of users, but independent on the radius  $D$ . When total number of users  $U$  in the system is higher, the optimal value of  $p_a$  is lower. After achieving its maximal value, the system throughput starts reducing with further increasing of  $p_a$ . This area holds for intensive load, thus the greater number of active users leads to increased cumulative OWC interference, which

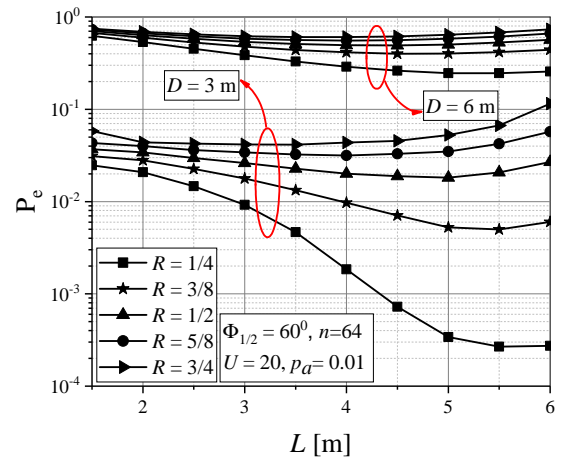


Fig. 3. Error probability vs.  $L$  for different values of rate  $R$ .

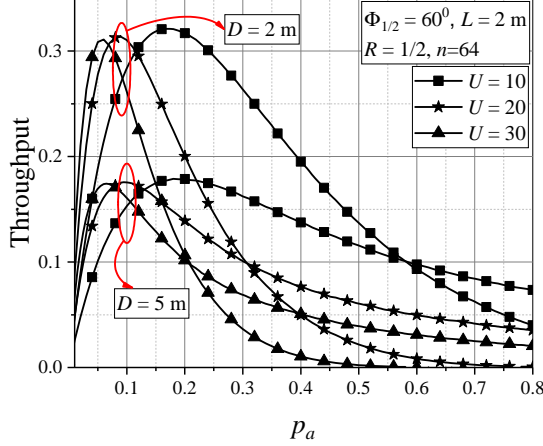


Fig. 4. Throughput vs.  $p_a$  for different number of IoT devices  $U$ .

results in deterioration of throughput performance.

Throughput dependence on the semi-angle at half illuminance  $\Phi_{1/2}$  is presented in Fig. 5 considering different values of activation probability. Increase of  $p_a$  up to a certain value will result in improving system. After that (value), throughput will continue to diminish with further increase of  $p_a$ . This proves that an optimal value of  $p_a$  exist for maximizing throughput performance of the system. Furthermore, Fig. 5 shows how throughput behaves for different values of  $\Phi_{1/2}$ . Depending on  $p_a$ , i.e., number of active OWC-based IoT devices, greater value of  $\Phi_{1/2}$  improve or degrade system performance. The semi-angle at half illuminance of LED determines Lambertian order of the LED source, or in other words, it determines the received optical signals intensities from IoT users at the OWC AP. When the value  $\Phi_{1/2}$  is greater, optical beam at LED sources output will be wider, thus the received power from the users far distant from the AP will be greater. This holds for all IoT devices, thus the semi-angle will have strong impact on both referent user and interference contribution (i.e., overall received SINR). To conclude, since  $\Phi_{1/2}$  represents important parameter which has impact on received optical signal intensity, the number of active users (and overall interference in that way) will decide if increase of  $\Phi_{1/2}$  will bring better or worse system throughput.

Fig. 6 shows the throughput dependence on the activation probability  $p_a$  for different values of maximal achievable rate  $R$ . As previously stated, greater rate brings improved system performance. Moreover, Fig. 6 also proves that optimal value of  $p_a$  occurs to achieve maximal value of the system throughput. From presented results it can be concluded that the optimal value  $p_a$  differs for different number of overall users, but it is the same regardless of the employed rate  $R$  in FBL based OWC scenario.

## VI. CONCLUSION

In this paper, we have analyzed an indoor OWC-based IoT system in finite-length regime. As a RA policy, the SA with capture effect has been adopted for uplink transmission,

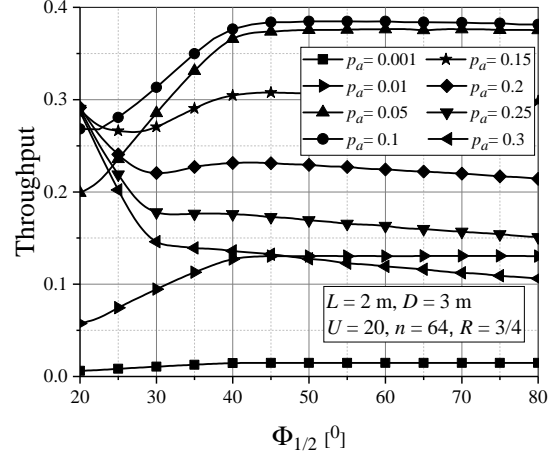


Fig. 5. Throughput vs.  $\Phi_{1/2}$  for different activation probability  $p_a$ .

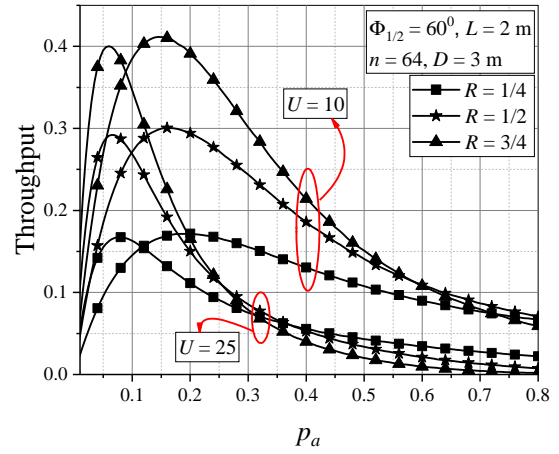


Fig. 6. Throughput vs.  $p_a$  for different number maximal achievable rate  $R$ .

meaning that the effect of the collisions introduced by the interference contribution has been taken into account while determining system performance. Based on the received SINR statistics, an analytical expression for the error probability in FBL regime has been derived, as well as overall throughput of system under investigation. Derived expressions were utilized to obtain numerical results, which are further used to analyze system performance behavior depending on the OWC channel model parameters.

Presented results have shown how the geometric setup of the OWC-based IoT system and the activation probability affect the error probability and throughput performance. It has been proven that the OWC-based system geometry has an significant impact on system performance, and should be taken into account during design of OWC-based IoT systems in order to assess and optimize the RA protocol performance.

## ACKNOWLEDGMENT

This work has received funding from the European Union Horizon 2020 research and innovation programme under the grant agreement No 856967 and by the Secretariat for Higher Education and Scientific Research of the Autonomous Province of Vojvodina through the project “Visible light technologies for indoor sensing, localization and communication in smart buildings” (142-451-2686/2021). This research was supported by the Science Fund of the Republic of Serbia, Program DIASPORA, #GRANT 6393139, AVIoTION and by the European Union COST Action CA19111.

## REFERENCES

- [1] M. Petkovic, T. Devaja, D. Vukobratovic, F. J. Escribano, and Č. Stefanović, “Reliability Analysis of Slotted Aloha with Capture for an OWC-based IoT system”, *2021 17th International Symposium On Wireless Communication Systems (ISWCS)*, pp. 1-6, 2021.
- [2] M. Z. Chowdhury, M. T. Hossan, A. , and Y. M. Jang, “A Comparative Survey of Optical Wireless Technologies: Architectures and Applications,” *IEEE Access*, vol. 6, pp. 9819-9840, 2018.
- [3] Z. Ghassemlooy, W. Popoola, and S. Rajbhandari, *Optical Wireless Communications: System and Channel Modelling With MATLAB*. Boca Raton, FL, USA: CRC Press, 2013.
- [4] Z. Ghassemlooy, L. N. Alves, S. Zvanovec, and M. A. Khalighi, (Eds.). *Visible Light Communications: Theory and Applications*. Boca Raton, FL, USA: CRC Press, 2017.
- [5] Z. Ghassemlooy, S. Arnon, M. Uysal, Z. Xu and J. Cheng, “Emerging Optical Wireless Communications-Advances and Challenges,” *IEEE J. Sel. Areas Commun.*, vol. 33, no. 9, pp. 1738-1749, Sept. 2015.
- [6] P. Popovski and M. Sidi, *Wireless Connectivity: An Intuitive and Fundamental Guide*. Springer Science & Business Media, 2020. Popovski, Peta
- [7] M. Berioli, G. Cocco, G. Liva, and A. Munari, *Modern random access protocols*, Foundations and Trends® in Networking, vol. 10, no.4, pp. 317-446, 2016.
- [8] R. Rom and M. Sidi, *Multiple access protocols: performance and analysis*. Springer Science & Business Media, 2012.
- [9] F. Clazzer, A. Munari, G. Liva, F. Lazaro, C. Stefanovic, and P. Popovski, “From 5G to 6G: Has the time for modern random access come?” in *Proc. 1st 6G summit*, Levi, Finland, Mar. 2019.
- [10] L. G. Roberts, “ALOHA packet system with and without slots and capture,” *ACM SIGCOMM Comput. Commun. Review.*, vol. 5, no. 2, pp. 28–42, 1975.
- [11] A. Munari, F. Clazzer, G. Liva, and M. Heindlmaier, “Multiple-relay slotted ALOHA: performance analysis and bounds,” *IEEE Trans. Commun.*, vol. 69, no. 3, pp. 1578–1594, 2021.
- [12] M. Zorzi, “Mobile radio slotted ALOHA with capture, diversity and retransmission control in the presence of shadowing,” *Wirel. Netw.*, vol. 4, no. 5, pp. 379–388, 1998.
- [13] M. S. Corson and A. Ephremides, “An analysis of multi-receiver, nonadaptive, slotted ALOHA with capture for wireless communications in factories,” in *Proc. IEEE INFOCOM 1993*, San Francisco, CA, USA, Mar. 1993, pp. 421–428.
- [14] Onozato, Yoshikuni, Jin Liu, and Shoichi Noguchi, “Stability of a slotted ALOHA system with capture effect,” *IEEE Trans. Vehicular Technology*, vol. 38, no. 1, pp. 31-36, 1989.
- [15] A. Gupta and X. Fernando, “Exploring Secure Visible Light Communication in Next-generation (6G) Internet-of-Things,” in *Proc. IWCMC 2021*, 2021, pp. 2090-2097.
- [16] S. S. Oyewobi, K. Djouani, and A. M. Kurien, “Visible Light Communications for Internet of Things: Prospects and Approaches, Challenges, Solutions and Future Directions,” *Technologies*, vol. 10, no. 1, 2022.
- [17] M. Z. Chowdhury, et al., “The role of optical wireless communication technologies in 5G/6G and IoT solutions: Prospects, directions, and challenges,” *Appl. Sci.*, vol. 9, no. 20, 2019.
- [18] A. Hamza and T. Tripp. “Optical wireless communication for the Internet of Things: Advances, challenges, and opportunities,” 2020, , doi: 10.36227/techrxiv.12659789.v1.
- [19] M. Haus, et al. “Enhancing indoor IoT communication with visible light and ultrasound,” in *Proc. ICC 2019*, Shanghai, China, 2019, pp. 1–6.
- [20] S. R. Teli, S. Zvanovec, and Z. Ghassemlooy, “Optical internet of things within 5G: Applications and challenges,” in *Proc. IOTAIS 2018*, Bali, Indonesia, 2018, pp. 40–45.
- [21] Chia-Wei Chen, et al. “Visible light communications for the implementation of internet-of-things,” *Opt. Eng.*, vol. 55, no. 6, 2016
- [22] D. Vukobratovic and F. J. Escribano, “Adaptive multi-receiver coded slotted ALOHA for indoor optical wireless communications”, *IEEE Commun. Lett.*, vol. 24, no. 6, pp. 1308 - 1312, June 2020.
- [23] L. Zhao, X. Chi, and W. Shi, “A QoS-driven random access algorithm for MPR-capable VLC system,” *IEEE Commun. Lett.*, vol. 20, no. 6, pp. 1239–1242, 2016.
- [24] L. Zhao, X. Chi, and S. Yang, “Optimal aloha-like random access with heterogeneous QoS guarantees for multi-packet reception aided visible light communications,” *IEEE Trans. Wireless Commun.*, vol. 15, no. 11, pp. 7872–7884, 2016.
- [25] T. Li, X. Chi, F. Ji, H. Shi, and S. Wang, “Optimal optical camera communication-ALOHA random access algorithm aided visible light communication system,” *Opt. Eng.*, vol. 59., no. 7, 2020.
- [26] Y. Polyanskiy, H. V. Poor, and S. Verdú, “Channel coding rate in the finite blocklength regime,” *IEEE Trans. Inf. Theory*, vol. 56, no. 5, pp. 2307–2359, May 2010.
- [27] J. M. Kahn and J. R. Barry, “Wireless infrared communications,” *Proc. of the IEEE*, vol. 85, no. 2, pp. 265-298, Feb. 1997.
- [28] M. Petkovic, D. Vukobratovic, A. Munari and F. Clazzer, “Relay-aided slotted aloha for optical wireless communications”, in *Proc. CSNDSP 2020*, Porto, Portugal, 2020.
- [29] A. Papoulis and H. Saunders, *Probability, random variables and stochastic processes*, 4th ed., McGraw Hill, 2002.
- [30] I. S. Gradshteyn and I. M. Ryzhik, *Table of Integrals, Series, and Products*. 6th ed., New York: Academic, 2000.
- [31] J. H. Curtiss, “On the distribution of the quotient of two chance variables,” *Ann. Math. Stat.*, vol. 12, no. 4, pp. 409-421, 1941.
- [32] J. Scarlett, V. Y. F. Tan, and G. Durisi, “The dispersion of nearest neighbor decoding for additive non-Gaussian channels,” *IEEE Trans. Info. Th.*, vol. 63, no. 1, pp. 81–92, Jan. 2017.
- [33] J. Park, “Rate analysis of ultra-reliable low-latency communications in random wireless networks,” arXiv preprint arXiv:1910.13868, 2019.